Journal Pre-proof

Accurate surface normal representation to facilitate gradient coil optimization on curved surface

Hao Ren, Hui Pan, Feng Jia, Jan G. Korvink, Zhenyu Liu

PII: S2772-5162(22)00019-5

DOI: https://doi.org/10.1016/j.mrl.2022.05.001

Reference: MRL 100042

To appear in: *Magnetic Resonance Letters*

Received Date: 15 February 2022

Revised Date: 5 May 2022

Accepted Date: 5 May 2022

Please cite this article as: H. Ren, H. Pan, F. Jia, J.G. Korvink, Z. Liu, Accurate surface normal representation to facilitate gradient coil optimization on curved surface, *Magnetic Resonance Letters*, https://doi.org/10.1016/j.mrl.2022.05.001.

CRediT author statement

Hao Ren: Methodology, Software->algorithm, Validation, Formal analysis, Investigation, Writing-Original Draft, Visualization.
Hui Pan: Methodology, Software->algorithm, Formal analysis, Investigation, Data Curation, Visualization.
Feng Jia: Methodology, Software->algorithm.
G.Korvink: Conceptualization, Writing-Review & Editing,.
Zhen-yu Liu: Conceptualization, Methodology, Software, Resources, Writing-Review & Editing, Supervision, Project administration.

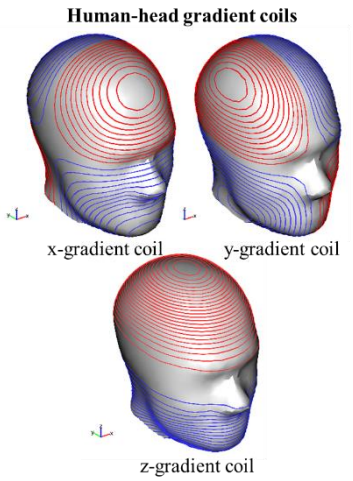

Magnetic Resonance Letters

Research Article

Accurate surface normal representation to facilitate gradient coil optimization on curved surface

Hao Ren [a, b], Hui Pan [b], Feng Jia [c], Jan G. Korvink [d, *], Zhenyu Liu [a, **]

[a] *Changchun Institute of Optics, Fine Mechanics and Physics, Chinese Academy of Sciences, Changchun, 130033, China*
[b] *School of Optoelectronics, University of Chinese Academy of Sciences, Beijing, 101499, China*
[c] *Department of Radiology, Medical Physics, Medical Center University of Freiburg, Faculty of Medicine, University of Freiburg, Freiburg, 79110, Germany*
[d] *Institute of Microstructure Technology, Karlsruhe Institute of Technology (KIT), Karlsruhe, 76049, Germany*

ABSTRACT

The design methods for gradient coils are mostly based on discrete extrinsic methods (e.g., the *Biot–Savart* integration calculation), for which the surface normal vector strongly influences any numerical calculation of the discretized surface. Previous studies are mostly based on regular or analytical surfaces, which allow normal vectors to be expressed analytically. For certain applications, design methods for extending current-carrying surfaces from developable or analytic geometries to arbitrary surfaces generated from a scanned point cloud are required. The key task is to correctly express the discretized normal vectors to ensure geometrical accuracy of the designed coils. Mathematically, it has been proven that applying a Delaunay triangulation to approximate a smooth surface can result in the discrete elemental normal vectors converging to those of the original surface. Accordingly, this article uses Delaunay triangulation to expand upon previous design methods so that they encompass arbitrary piecewise continuous surfaces. Two design methods, the stream function and the so-called solid isotropic material with penalization (SIMP) method, are used to design circumvolute and noncircumvolute gradient coils on general surfaces.

Keywords: gradient coils, Delaunay triangulation, stream function, SIMP method

1. Introduction

As one of the most popular medical imaging and diagnosis methods, magnetic resonance imaging (MRI) can reveal the physiological hierarchy of an organism, as well as biochemical features at the molecular level, thereby providing detailed and

* Corresponding author.
** Corresponding author.
E-mail addresses: jan.korvink@kit.edu (J. Korvink), liuzy@ciomp.ac.cn (Z. Liu).
Peer review under responsibility of Innovation Academy for Precision Measurement Science and Technology (APM), CAS.

accurate images of various sections. Compared with other medical imaging methods (e.g., computed tomography, X-ray, B-scan ultrasonography), MRI is more discriminatory and does not emit ionizing radiation.

One of the main components in an MRI system is gradient coil,which is used to form orthogonal magnetic field gradients within the imaging volume, enabling the frequency and phase encoding of a magnetization that is linearly proportional to the magnetic field strength. The main design goals for gradient coils are the gradient field uniformity, and the strength of the field gradient. Usually, the uniformity of the gradient magnetic field enables an undistorted MRI image, and stronger gradients allow for higher resolution of the resulting MRI images.The ideal z-direction component of gradient magnetic field B_z in the imaging volume satisfies a linear distribution. Most existing MRI gradient coils use developable surfaces (e.g., cylinders) to carry the electric current. The efficiency of these coils can be improved by placing an irregular current-carrying surface close to the object under inspection. In practical applications, the magnetization deviations over a uniform phantom are used to measure the actual quality of gradient magnetic fields. Typically, the maximum inaccuracy must be less than 5% to prevent excessive imaging distortion.

The gradient coil design defines an inverse mathematical problem. For MRI systems, the current is usually confined to a current-carrying surface, and its required distribution is inversely determined by the magnetic field gradient preset at the region of interest (ROI). Inverse design methods mainly include the target field [1-6], the stream function [7-10] methods, and the solid isotropic material based on the penalization (SIMP) method especially for microscale gradient coils [11].

At present, most MRI gradient coil designs are based on smooth developable surfaces whose normals can be accurately calculated. For example, on a biplane (or cylinder), the coils spread out into the coordinate plane (Fig. 1). But dedicated MRI systems (e.g., a system dedicated to imaging the human head, or a spherical surface for imaging cells) require coils to be placed on more complex surfaces. On curved surfaces, the tangential gradient operator must be used, the accuracy in calculating the current density and gradient on a surface depends on the normal vectors. The accuracy of the normal for a discrete surface ultimately affects the imaging quality. At the same time, irregular smooth surfaces often require densely sampled point clouds and triangular meshes to construct computer models. In these models, numerous redundant sampling points and poor-quality triangulations may present. When these surfaces are used as the calculation models, it is necessary to select a valid subset of nodes and reconstruct good triangulations. Therefore, a mesh simplification algorithm is needed for a given 3D structure. A general case in which a surface without analytic expression (i.e., normal vectors on the irregular surface cannot be described analytically) is constructed using dense cloud points is considered in this study.

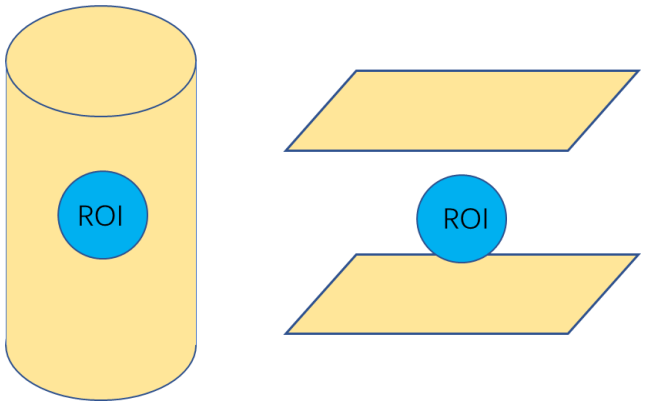

Fig. 1. Cylindrical and biplanar current-carrying surfaces

Calculation errors in magnetic induction can arise when existing gradient coil designs are directly applied to arbitrary surfaces. This can result in further imaging distortions. Therefore, it is important to ensure that the magnetic induction is accurately calculated from the normal. This article introduces methods for designing gradient coils on arbitrary surfaces. We achieved this by extending the stream function and SIMP method for gradient coils on these surfaces. Furthermore, we show that the gradient coils are accurate and satisfy the design requirements. Moreover, the key factors affecting the accuracy of the designed gradient coils are investigated, and we discuss the necessary methodology.

2. Discretization of irregular design surface

The magnetic induction intensity at any point in space can be calculated using the *Biot–Savart* formula:

$$\boldsymbol{B}(\boldsymbol{r}) = \frac{\mu}{4\pi}\int_S \frac{\boldsymbol{J}(\boldsymbol{r}')\times|\boldsymbol{r}-\boldsymbol{r}'|}{|\boldsymbol{r}-\boldsymbol{r}'|^3}\mathrm{d}S \tag{1}$$

Here, $\boldsymbol{J}$ is the current density, $\boldsymbol{r}'$ is the position vector of the current density, $\boldsymbol{r}$ is the position vector of the objective point, $\boldsymbol{B}$ is magnetic induction, S is current carry surface and μ is the vacuum permeability. Fig. 2 shows a schematic of the gradient coil setup, indicating the ROI and conductor surface.

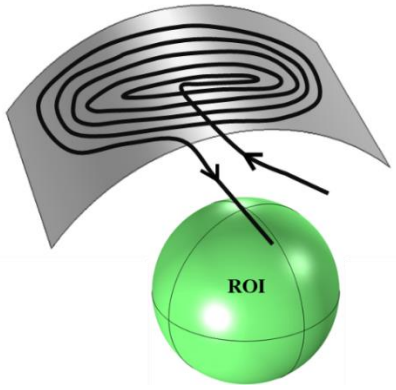

Fig. 2. Schematic of a gradient coil arrangement, showing the conductor surface with a coil pattern, and the region of interest (ROI).

The design and optimization of gradient coils is a mathematical problem. When the linear gradient magnetic field in the ROI corresponds to an ideal field distribution, the current density distribution (conductor configuration) that produces the target magnetic field will be found on a specified current-carrying surface. The main numerical analysis and calculation methods used to solve the inverse problem of finding the electromagnetic field values are the stream function and SIMP method. These are based upon the idea of discretizing a surface model via triangular or quadrilateral elements. Therefore, approximation errors for the numerical solutions of the two gradient coil design methods primarily depend upon the quality of the surface mesh. The accuracy of a surface mesh depends on whether the discrete normal vectors and area of the polyhedral mesh converge to the original surface. Hence, we first discuss the effects of discrete surfaces and the effectiveness using a Delaunay triangulation method of meshing a current-carrying surface to obtain accurate simulation results.

2.1 Discrete normal vectors of piecewise continuous surface

Each point on the continuous surface has its corresponding normal vector. On discrete surfaces, because the tangential gradients on the nodes are required, the normal vectors on the nodes must be calculated. The normal vector on a node represents the average of the normal vectors of all elements connected to that node.

2.2 Approximation of discrete surface mesh

The present article focuses on surface triangulations, which can be used to discretize a wide variety of complex surfaces. Essentially, surfaces embedded in Euclidean space are triangulated to approximate smooth surfaces using a discrete triangular mesh. This problem can be divided into two parts:

(I) Select the appropriate mesh nodes on the smooth surface.

(II) Appropriately triangulate the selected nodes.

During triangulation of a smooth surface, the use of more discretized nodes and elements will not always guarantee that the discrete surface approximates the smooth surface. The famous *lampion de Schwarz* is a typical example [17] (see Fig. 3). Let *C* be a cylinder of finite height *H* and radius *R*. Let *P(n, N)* denote the triangulated mesh whose nodes S_{ij} belong to *C* and are defined as (*n*, *N* are the positive integers)

$$\forall\ i \in \{0, \dots, n\}, \forall\ j \in \{0, \dots, N\},$$

$$S_{i,j} = (R\ \cos\ i\alpha, R \sin i\alpha, jh)\ \text{ if } j \text{ is even},$$

$$S_{i,j} = (R\cos(i\alpha + \alpha/2), R\sin(i\alpha + \alpha/2), jh)\ \text{ if } j \text{ is odd},$$

and whose faces are

$$S_{i,j}S_{i+1,j}S_{i,j+1},\ \text{and}$$

$$S_{i,j}S_{i-1,j+1}S_{i,j+1}$$

where $\alpha = 2\pi/n$ and $h = H/N$. For example, when n tends to infinity, the area $\mathcal{A}(P(n,n^3))$ of $P(n,n^3)$ tends to infinity and the normals of $P(n,n^3)$ tend to be orthogonal to the normals of surface *C*. The Hausdorff distance of the *lampion de Schwarz* surface to the smooth surface *C* is zero in this limit. Furthermore, the area of the discrete surface, its discrete Gaussian curvature, and its discrete mean curvature, do not converge to those of the original smooth surface. In a scenario where this type of mesh is applied to numerical calculations of physical problems, the discretization errors in the normals and triangle areas will result in unacceptable numerical errors.

(a) (b)

Fig. 3. *Lampion de Schwarz*: (a) $n = 5$, discretion of the cylindrical surface; (b) $n = 8$, discretion of the cylindrical surface.

To approximate a smooth surface using the discretization, the surface triangulation must satisfy two conditions [18]:

(a) Discrete surface normals converge to the smooth surface's normal field.

(b) The Hausdorff distance converges to zero.

These two conditions guarantee that the area and curvature of the discrete surface converge to the smooth surface. Therefore, to obtain a good surface mesh, it is necessary to make some restrictions in the form of the triangulation: when the number of nodes tends to infinity, the maximum edge length of all triangles tends to zero, and the minimum angle of all triangles exceeds a threshold [19].

2.3 Delaunay triangulation

For a set of nodes on a surface, there exists only one unique triangulation such that the sum of minimum angles for all triangular elements is the largest among all triangulations. This is called the Delaunay triangulation. This triangular mesh satisfies conditions (a) and (b) mentioned above.

The surface constructed by cloud points should first be meshed with Delaunay triangles. To increase the smoothness of the solution, higher-order elements or splines can be used. Numerous methods can be used to obtain a Delaunay triangulation. Here, we use a method called the farthest point sampling method, which is based on the fast marching method [20].

The associated Voronoi diagrams are fundamental data structures. They have been

extensively studied in the field of computational geometry. Given a finite set of points in a plane, the triangulation whose angular vector is maximal for the lexicographical order forms a Delaunay triangulation, which is defined as the dual of the Voronoi diagram (Fig. 4) [21]. The Voronoi diagram is generated using the fast marching method, and it can determine how nodes are linkede. Each node in a Voronoi cell is linked to nodes in an adjacent cell such that each node always links to several nodes with shorter Euclidean distances; furthermore, if the diagonals of the convex quadrilaterals formed by any four adjacent nodes are interchanged, the smallest of the six angles of the two triangles is reduced (Fig. 5).

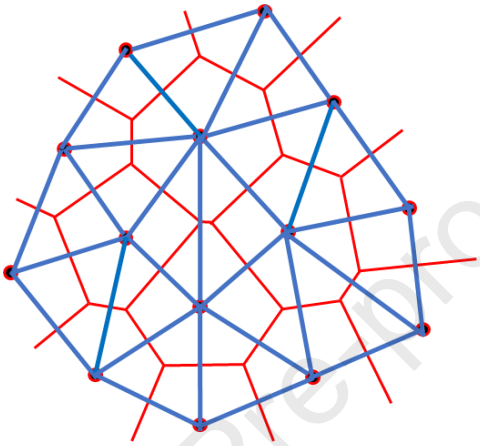

Fig. 4. Voronoi diagram (red) and its corresponding Delaunay triangulation (blue).

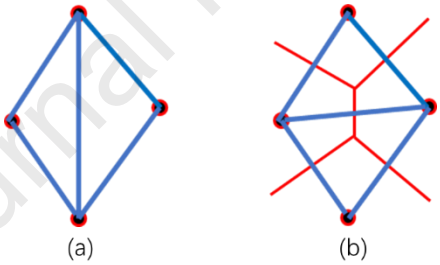

Fig. 5. Voronoi diagrams determine how nodes are connected to produce a Delaunay triangulation: (a) Arbitrary connections between nodes, which can cause poor triangulation; (b) A Voronoi diagram, which determines how nodes are connected.

In the Riemannian manifold, the shortest distance between two points is called the geodesic distance. Similar to the 2D plane scenario, the fast marching method for a surface is used to obtain the geodesic distance between nodes and to determine how they are linked. This method is used to answer Question II proposed in Section 2.2. It indicates that an edge is present between two nodes.

Many methods are available to answer Question I (proposed in Section 2.2). This article uses the farthest point sampling method proposed by G. Peyré et al. [22], for which an open-source MATLAB code has been published online. The nodes chosen in this method have a more even global distribution. The basic algorithmic steps for generating the mesh are shown in Fig. 6. The algorithm is used in this article for the surface meshing of subsequent gradient coil designs.

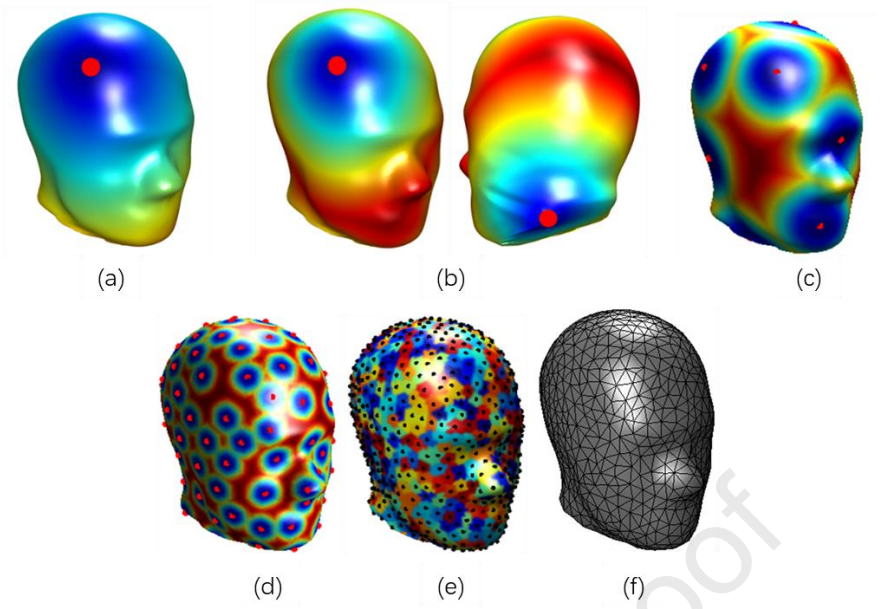

Fig. 6. The process of the farthest point sampling algorithm for generating a mesh: First, a set of dense sample vertexes are chosen to express a closed surface in the computer representation. Then, a vertex is randomly chosen as the first node for the mesh, and the fast marching algorithm is used to obtain a geodesic distance map on the surface. Next, a second node is chosen as the longest geodesic distance vertex. A third node is chosen along the longest geodesic distance to the other two nodes. This step is then repeated until the number of nodes satisfies the requirements or the minimum geodesic distances between nodes are less than a given value. Finally, the fast marching algorithm is applied again to obtain the Voronoi diagram, and the Delaunay triangulation is obtained. (a) The first node (red node) and its geodesic distance map. (b) The first two nodes (another node on the back) and their shortest geodesic distance map. (c), (d) More nodes are chosen. (e) Voronoi diagram. (f) Delaunay triangulation.

2.4 Spherical surface mesh example

An example of a spherical current-carrying surface is considered as a benchmark to verify the accuracy of the numerical calculations using the Delaunay triangular mesh. The center of the sphere is located at the origin O. Let $\psi = \alpha z$ on the surface (z is the z-direction coordinate), where α is a constant. The magnetic induction B_z at point O can then be derived, this is a constant equal to $\frac{2}{3}\alpha\mu_0$ [See Appendix A], where μ_0 is the vacuum permeability.

The accuracy of the *Biot–Savart* numerical integration process that uses normal vectors on a discrete spherical surface will converge to its true value when the number of nodes increases. Fig. 7 shows the Delaunay triangulation for the spherical surface. The horizontal axis of Fig. 8 represents the number of nodes on the spherical surface. The vertical axis of Fig. 8(a) denotes the error rate between the numerical integration of the spherical area and the theoretical value. The vertical axis of Fig. 8(b) denotes the error between the numerical integration of the magnetic induction intensity and the theoretical value, both evaluated at the center of the sphere. This shows that, when the number of nodes increases, the numerical integral of the discrete surface gradually approaches its theoretical value. The vertical axis of Fig. 8(c) is the angular error of the

direction of the discrete normal, which lies between the element normal and the mean normal of its corresponding surface triangle.

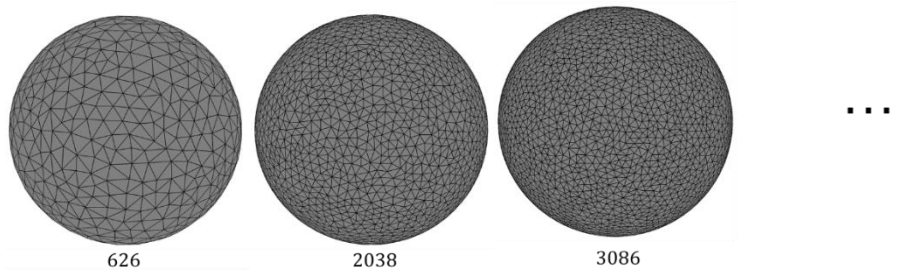

Fig. 7. Delaunay triangulation for the spherical surface.

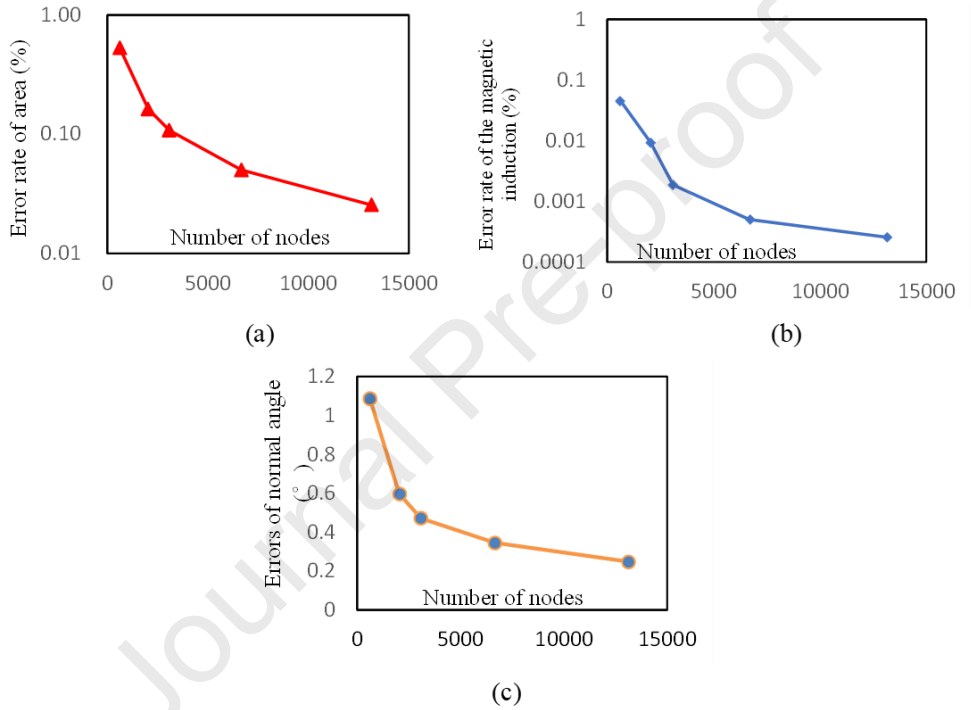

Fig. 8. When the number of nodes increases, the numerical results converge to their theoretical value. Here, we show the remaining errors for (a) area, (b) magnetic induction, and (c) normal angle.

3. Design methods

Rather than using an electrical current as the design variable, it is simpler to choose a scalar field quantity during the optimization of gradient coils. The current density inside an electrostatic field is irrotational and solenoidal. Therefore, two scalar functions ψ and φ can be derived as variables, where ψ is defined as the stream function and φ is the potential function (electrical potential). In this study, the stream function and SIMP method are primarily used, where the design variables are ψ and φ, respectively. For both of the stream function method and the SIMP method, the tangential gradient operator ∇_Γ is defined to calculate the gradient of a scalar field on a surface Γ [15-16] or manifold. For a 2D curved surface $\Gamma \in \mathbb{R}^2$ embedded in

Euclidean space $\mathbb{R}^3$, the variable tangential derivative represents the Cartesian components of the tangential projection of the variable gradient, and the components in three directions are calculated as

$$\nabla_\Gamma u = \nabla u - \nabla u \cdot \boldsymbol{n}^T \boldsymbol{n} = \left(u_{tx}, u_{ty}, u_{tz}\right) \tag{2}$$

where u represents a certain scalar quantity, $\nabla u = (\partial u/\partial x, \partial u/\partial y, \partial u/\partial z)$, and $\boldsymbol{n}$ is normal to the surface, components of the tangential gradient in three directions of the Euclidean space will be represented in the form of $\left(u_{tx}, u_{ty}, u_{tz}\right)$.

3.1 Stream function method on surfaces

The stream function method[8] solves the inverse problem by changing the vector variables to scalar ones, which greatly simplifies the current density optimization. The electrical current on the current-carrying surface satisfies the continuity equation for the electrostatic field:

$$\nabla_\Gamma \cdot \boldsymbol{J} = 0 \tag{3}$$

Here, $\boldsymbol{J}$ is the current density on surface Γ. According to Eq. (3), the stream function ψ is defined by

$$\boldsymbol{J} = \nabla_\Gamma \psi \times \boldsymbol{n} \tag{4}$$

where $\boldsymbol{n}$ is the normal of the current-carrying surface.

3.1.1 Calculation of basic physical quantities

After the surface is discretized, each element can be approximated as a plane whose local normal vector is

$$\boldsymbol{n_e} = \left(n_{xe}, n_{ye}, n_{ze}\right) \tag{5}$$

By substituting Eq. (5) into Eq. (4), one obtains

$$\begin{aligned}\boldsymbol{J} &= \nabla_\Gamma \psi \times \boldsymbol{n_e} \\ &= \begin{vmatrix} \boldsymbol{i} & \boldsymbol{j} & \boldsymbol{k} \\ \psi_{tx} & \psi_{ty} & \psi_{tz} \\ n_{xe} & n_{ye} & n_{ze} \end{vmatrix} \\ &= \left(n_{ze}\psi_{ty} - n_{ye}\psi_{tz}\right)\boldsymbol{i} + \left(n_{xe}\psi_{tz} - n_{ze}\psi_{tx}\right)\boldsymbol{j} \\ &\quad + \left(n_{ye}\psi_{tx} - n_{xe}\psi_{ty}\right)\boldsymbol{k}\end{aligned} \tag{6}$$

Typically, we take the magnetic induction B_0 to be in the z-direction (i.e., B_z). According to the *Biot–Savart* integral, the magnetic induction intensity in the *z* direction is generated by an electrical current on a curved surface in space, according to

$$B_z = \frac{\mu_0}{4\pi} \int_S \frac{J_y(x - x_0) - J_x(y - y_0)}{\left((x - x_0)^2 + (y - y_0)^2 + (z - z_0)^2\right)^{3/2}} \mathrm{d}S \tag{7}$$

where J_x and J_y are the components of current density in the x and y directions, respectively; (x_0, y_0, z_0) is the coordinate of the magnetic field point; and S is the current-carrying surface. Using Eqs. (6) and (7) and calculating the z-direction magnetic induction, B_{zk} is generated using the current density on each element surface S_e:

$$B_{zk} = \frac{\mu_0}{4\pi}\int_{Se} \frac{(n_{xe}\psi_{tz} - n_{ze}\psi_{tx})(x_k - x_0) - (n_{ze}\psi_{ty} - n_{ye}\psi_{tz})(y_k - y_0)}{((x_k - x_0)^2 + (y_k - y_0)^2 + (z_k - z_0)^2)^{3/2}} \mathrm{d}S_e \quad (8)$$

Thus, the z-direction magnetic induction at a point in space represents the scalar sum of all element contributions, expressed as

$$B_{z,s} = \sum_{k=1}^{n} B_{zk} \quad (9)$$

where n is the number of elements.

3.1.2 *Optimization model and calculation*

The smooth surface is discretized into several triangular elements, and Lagrange linear interpolation is performed on the stream function values of m nodes on the surface:

$$\psi = \sum_{i=1}^{m} \psi_i N_i \quad (10)$$

Here, the shape function N_i varies along with a set of interpolation coefficients.

When uniform sampling is conducted on points in the gradient magnetic field of the ROI, each of the number of samples p has an ideal value. The least-squares approximation of the ideal value (and the actual value) is made to minimize the residual; this is used as the objective function of the optimization:

$$\min: F_0 = \sum_{s=1}^{p} \frac{1}{2}\left(B_{z,s} - B_{z,s}^*\right)^2 \quad (11)$$

Here, $B_{z,s}^*$ is the ideal magnetic induction of the sampling points.

To find the local minimum value of the residual, the first-order partial derivative of the objective function is set to zero, where $(\psi_1, \psi_2, \ldots, \psi_m)$ satisfies the following equation:

$$\frac{\partial F_0}{\partial \psi_i} = \sum_{s=1}^{p} \left(B_{z,s} - B_{z,s}^*\right)\frac{\partial B_{z,s}}{\partial \psi_i} = 0 \quad (12)$$

Using Eq. (8), (9), and (10):

$$\frac{\partial B_{z,s}}{\partial \psi_i} = \sum_{k=1}^{n} \frac{\mu_0}{4\pi}\int_{Se} \frac{\left(n_{xe}\frac{\partial N_{i,tz}}{\partial \psi_i} - n_{ze}\frac{\partial N_{i,tx}}{\partial \psi_i}\right)(x_k - x_0) - \left(n_{ze}\frac{\partial N_{i,ty}}{\partial \psi_i} - n_{ye}\frac{\partial N_{i,tz}}{\partial \psi_i}\right)(y_k - y_0)}{((x_k - x_0)^2 + (y_k - y_0)^2 + (z_k - z_0)^2)^{3/2}} \mathrm{d}S_e \quad (13)$$

By solving the above linear equations, the value of the variable ψ at each node can be obtained. This is an ill-posed problem; hence, it needs to be supplemented by a regularized auxiliary objective function to improve the smoothness of the coil configuration [23].

3.2 SIMP method on surfaces

The SIMP method is a numerical optimization algorithm, which was first utilized in solid mechanics to design lightweight stressed components [12-13]. It was subsequently used to design the fluid flow path of flexible materials [14]. The SIMP method has also been used to design and optimize gradient coils on a cylindrical surface (developable surface) [11].

Compared to the stream function method, patterned gradient coils designed using the SIMP method do not contain multiturn wire windings. Thus, it is possible to effectively reduce the required length of the gradient coils and reduce the size of the magnetic resonance system. Moreover, this makes these systems easier to manufacture and more suitable for microscale MRI systems.

The purpose of the SIMP method is to identify the optimal material distribution that maximizes or minimizes the objective function within the design domain. Using finite element methods (FEMs), the distribution of conductive material on a current-carrying surface can be found by considering the gradient coil configuration. The fundamental equation of the SIMP method applied to an electrostatic field is the Laplace equation:

$$\nabla_\Gamma \cdot (\sigma \nabla_\Gamma \varphi) = 0 \tag{14}$$

Here, σ is the conductivity of the current-carrying material. According to finite element theory, when designing gradient coils using the SIMP method, the weak form of Laplace equation for the electrostatic field [Eq. (14)] on the surface Γ is

$$\int_{\Omega_\Gamma} \sigma \nabla_\Gamma \varphi \cdot \nabla_\Gamma v \mathrm{d}\Omega - \int_{\ell_N} v \frac{\partial \varphi}{\partial \boldsymbol{n}_\ell} \mathrm{d}\ell = 0 \tag{15}$$

where σ is the conductivity, φ is the scalar electric potential function, v is the weight function of the potential function φ, Ω indicates the design domain (solution domain), ℓ_N denotes the Neumann boundary, ℓ is the boundary with the Neumann condition and $\boldsymbol{n}_\ell$ denotes the normal of the boundary curve.

This study extends the SIMP method from developable to nondevelopable surfaces. This will enable us to consider gradient coils targeting the outer surface of a biological cell, which is mostly nondevelopable. Certain cells have shapes similar to a spherical or closed surface; hence, we will consider this simpler case.

3.2.1 Surface electrostatic field

The resistive electrostatic field on a surface satisfies the Laplace equation in Eq.(14). The boundary conditions of Eq.(14) are as follows: the insulation boundary ℓ_N: $\partial\varphi/\partial\boldsymbol{n}_\ell = 0$; the potential input boundary ℓ_{in}: $\varphi = \varphi_0$; the grounding boundary ℓ_g:

$\varphi = 0$.

The z-direction component of the magnetic induction for a point (x_0, y_0, z_0) in the ROI is expressed by the current density in Eq. (7). The SIMP method yields a solution to the optimization problem. This optimization problem is ill-conditioned. The Laplace equation, as a constraint condition, ensures the continuity of the electric current in the electrostatic field. In the solution of regular problems, σ is a constant, and φ is a definite numerical solution. However, in the optimization procedure, the value of σ is dependent on an optimization variable ρ; each iteration step determines a value of σ [through optimization algorithms such as the method of moving asymptotes (MMA) or optimality criterion (OC)] and then solves the Laplace equation to obtain the numerical solution of φ. Thus, for the electrostatic field, the presence or absence (conductivity) of conductive material is represented by the value of ρ. If the value of ρ on a node is equal to 1, a conductor is present. If the value of ρ on a node is equal to 0, no conductor is present. To make the value of ρ maximally satisfy the 0–1 distribution (without expressing an intermediate value), the conductivity of the conductive material is expressed via the SIMP interpolation method [24,25]:

$$\sigma(\rho) = \sigma_A + (\sigma_C - \sigma_A)\big(\rho(x)\big)^p \tag{16}$$

In Eq. (16), $\sigma_C = 5.99 \times 10^7$ S/m is the conductivity of the copper material, $\sigma_A = 5 \times 10^{-15}$ S/m is the conductivity of air (insulation), p is a penalty factor (whose value range is 1–5), which is typically set equal to 3 in this problem in order to obtain a useable result [11].

Discrete surfaces that use Lagrange linear elements for each node exhibit two degrees of freedom: the optimization variable ρ and electric potential φ. These two variables are expressed on the surface of an electrostatic field as

$$\rho(x) = \sum_{i=1}^{n} N_i \rho_i \tag{17}$$

$$\varphi(x) = \sum_{i=1}^{n} N_i \varphi_i \tag{18}$$

where n is the total number of nodes used to discretize the surface. The two variables are taken into the discrete form of the finite element Poisson equation via a weighted residual approach, and the weight function v is taken as a set of base functions $(v_1, v_2, v_3, \dots, v_n) = (N_1, N_2, N_3, \dots, N_n)$, resulting in

$$\sum_{i=1}^{n} \varphi_i \int_{\Omega} \sigma(\rho) \nabla_{\Gamma} N_i \cdot \nabla_{\Gamma} N_j \mathrm{d}\Omega$$

$$= \int_{\ell_N} N_j \frac{\partial \varphi}{\partial \boldsymbol{n}_{\boldsymbol{\ell}}} \mathrm{d}\ell + \sum_{j=n+1}^{n+\partial n} \varphi_j \int_{\Omega} \sigma(\rho) \nabla_{\Gamma} N_i \cdot \nabla_{\Gamma} N_j \mathrm{d}\Omega \tag{19}$$

where (j = 1,2, 3…, n). Equation (19) is written in matrix form as

$$\boldsymbol{K\Phi} = \boldsymbol{P}, \tag{20}$$

where $\boldsymbol{\Phi} = (\varphi_1, \varphi_2, \varphi_3, \dots, \varphi_n)^T$; $\boldsymbol{K}$ is the stiffness matrix, with $K_{ij}^e =$

$\int_{\Omega_e} \sigma(\rho)\nabla_\Gamma N_i \cdot \nabla_\Gamma N_j \mathrm{d}\Omega_e$; and $\boldsymbol{P}$ is the voltage boundary condition vector of the electrostatic field on the surface. According to the electric potential $\varphi(x)$ and the equation $-\nabla_\Gamma \varphi = \boldsymbol{E}$ (electric field intensity), the electric current density $\boldsymbol{J}(\boldsymbol{x})$ can be obtained as

$$\boldsymbol{J}(\boldsymbol{x}) = \sigma(\rho)\nabla_\Gamma \varphi(x) = \sigma(\rho)\sum_{i=j}^{n} \nabla_\Gamma \varphi_j N_j$$

$$= \left(\sigma(\rho)\sum_{i=j}^{n} \varphi_j N_{j,tx}, \sigma(\rho)\sum_{i=j}^{n} \varphi_j N_{j,ty}, \sigma(\rho)\sum_{i=j}^{n} \varphi_j N_{j,ty} \right)$$

$$= \left(J_x, J_y, J_z\right). \tag{21}$$

Correspondingly, Eq. (21) is inserted into Eq. (7) to yield the z-direction component of the magnetic induction at a point (x_0, y_0, z_0) in the ROI:

$$B_{z,s} = \frac{\mu}{4\pi}\sigma(\rho)\int_\Omega \frac{\sum_{i=j}^{n} \varphi_j N_{j,ty}(x - x_0) - \sum_{i=j}^{n} \varphi_j N_{j,tx}(y - y_0)}{((x - x_0)^2 + (y - y_0)^2 + (z - z_0)^2)^{3/2}} \mathrm{d}\Omega \tag{22}$$

3.2.2 Optimization model and calculation

The optimization objective function minimizes the gradient field inaccuracy. Thus, the difference between the ideal gradient magnetic field and the generated gradient magnetic field should vanish. The magnetic induction intensity of the m points in the ROI is $\boldsymbol{B_{z,s}}$(s = 1, 2, 3, …, m); in vector form, this is $\boldsymbol{B_z} = (B_{z,1}, B_{z,2}, B_{z,3}, \ldots, B_{z,m})^T$. The ideal magnetic induction at all sampling points is $\boldsymbol{B_z^*} = (B_{z,1}^*, B_{z,2}^*, B_{z,3}^*, \ldots, B_{z,m}^*)^T$; hence, the main objective function is expressed as

$$\min: F_0 = \frac{1}{2}\sum_{s=1}^{m}(B_{z,m}^* - B_{z,m})^2 \tag{23}$$

When using only one objective function, non-convex least squares objective functions may suffer from bad optimization procedures. This makes it difficult to produce ideal results; hence, an auxiliary objective should be added to the objective function; for instance, that of minimizing the resistance

$$\min: F_1 = \frac{1}{G} \tag{24}$$

where G represents the conductance. Finally, the combined expression for the SIMP method on a surface is:

$$\min: f = F_0(\varphi, \rho) + \beta F_1$$

$$s.t. \qquad \boldsymbol{K\Phi} = \boldsymbol{P},$$

$$\sum_{i=1}^{n} \rho_i \mathrm{Vol}_i \le \mathrm{Vol}_\Omega^*, \tag{25}$$

$$0 \le \rho \le 1,$$

where $\sum_{i=1}^{n} \rho_i \mathrm{Vol}_i \le \mathrm{Vol}_\Omega^*$ is the volume fraction constraint for the conductive material, $\mathrm{Vol}_i = \int_\Omega N_i d\Omega$ is the volume fraction of each node, Vol_Ω^* is the upper limit of the sum of the volume fractions of all nodes, and β is the weight coefficient of the auxiliary object.

Before optimization, it is necessary to calculate the sensitivity of the objective function with respect to the design variables, because the SIMP method typically uses a gradient optimization algorithm. For multivariate sensitivity calculations, the adjoint method is applied. The specific calculation method is described in Ref. [11].

After the optimization model is established and the formula for calculating the sensitivity is derived, the optimization algorithm is used to evolve the variables. The OC method [26] or MMA [27] optimization algorithm can be used to design the gradient coils via the SIMP method. The entire optimization algorithm program applies the following steps when performing each iteration:

1. Calculate the distribution of the electric potential according to a set of boundary conditions and the distribution of the conductive material.
2. Calculate the objective function value according to the electrical potential distribution obtained in the previous step.
3. Calculate the sensitivity of each objective function for the design variables. The sensitivity can be processed via filtering to prevent checkerboard responses [28].
4. Use the optimization algorithm (OC or MMA) to evolve the values of the design variables. Similarly, the optimized design variables can be filtered to smoothen their distribution.
5. Check for convergence of the design; if it has converged, or a prespecified number of iteration steps have been executed, stop the iteration process.
6. If not converged, replace the original design variable value with the optimized design variable value and repeat the iteration from Step 1.

4. Numerical examples

The two design methods have their own advantages and disadvantages, which make them suitable in different situations. As mentioned in Section 1, the SIMP method is more suitable for microscale imaging systems (which have limited space in which to locate the gradient coil). Macroscale-device head imaging suffers from almost no manufacturing difficulties for multiple round coils. Therefore, the stream function method is applied for the head imaging of MRI. As stated above, to improve the coil efficiency, the shape of the current-carrying surface should be selected as close as possible to the objective. Therefore, the SIMP method examples in this paper use a spherical surface that resembles the shape of the cell, and the stream function method examples use the human-head surface.

4.1 Stream function method

4.1.1 Accuracy verification

The stream function method (using the discrete normal vector) is applicable to both the developable analytic and general discretized surfaces. To compare the accuracy of the algorithm, this method was used to obtain *x*- and *z*-gradient coils on a cylindrical current-carrying surface with a diameter of 0.7 m and a height of 1.5 m. The ROI was a spherical domain with a diameter of 0.35 m (Fig. 9), and the gradient value was 0.05 T/m. The design of the coils was essentially the same as that of *x*- and *z*-gradient coils, which were previously obtained using an unfolding plane method [29]. The maximum inaccuracy is used to represent the maximum error between the ideal and actual value of the magnetic induction intensity in ROI. Here, the maximum inaccuracy of the *x*-gradient coils obtained by the new method was 1.6133%, whilst the previous method was 1.6183%. The maximum inaccuracy of the *z*-direction gradient coils obtained by the new method was 1.4942%, while the previous method was 1.4982%. The two *x*-gradient coils were used to calculate the magnetic induction B_z at the point (0,0,0), achieving 0.02691 and 0.02713, respectively.

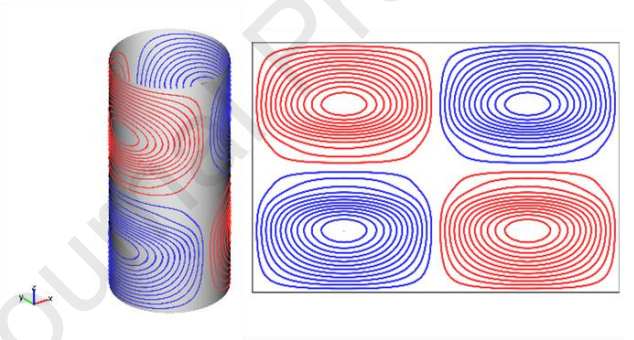

(a)

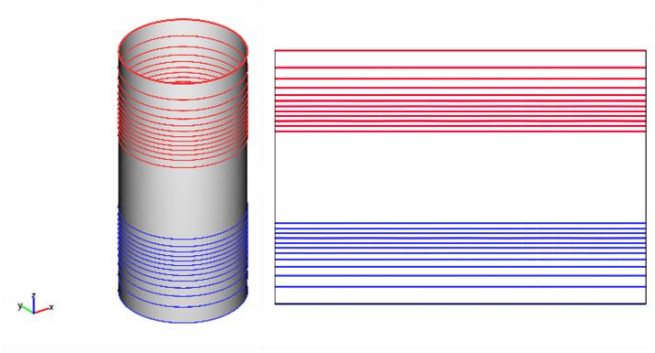

(b)

Fig. 9. Comparison of the wire configuration of gradient coils on a cylindrical surface: (a) Comparison of *x*-gradient coil results and (b) comparison of *z*-gradient coil results. (Left: the results obtained in this article; right: the results obtained in Ref. [29])

4.1.2 Examples of human-head surface

The stream function method can be used to design gradient coils for an MRI device confined to an arbitrary surface, such as that of a human head. The human-head surface (provided by COMSOL software) was first meshed using Delaunay triangles (Fig. 10).

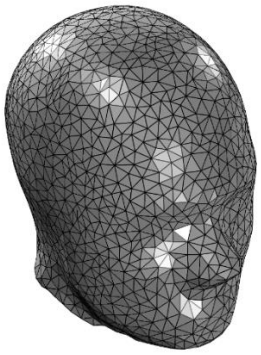

Fig. 10. Delaunay triangulation of a human-head surface.

The ROI is a spherical domain with a 5 cm radius inside the head surface (Fig. 11). 997 points were selected and evenly distributed inside the ROI as sampling points. We used the z-direction magnetic induction value $B_z = G_z \cdot z_0$, the y-direction magnetic induction $B_z = G_y \cdot y_0$, and the x-direction magnetic induction $B_z = G_x \cdot x_0$, with a maximum gradient value of 0.05 T/m.

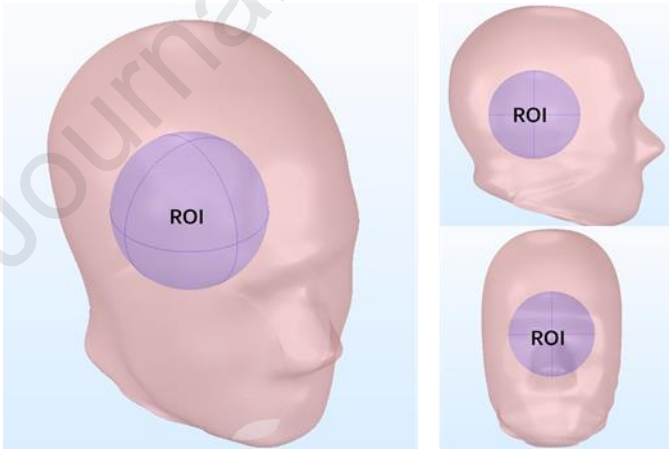

Fig. 11. ROI position.

The deviation from the target value was used to evaluate the accuracy of the magnetic fields for the generated gradient coils. For MRIs, the gradient magnetic field inaccuracy should be less than 5%. To generate a smooth continuous coil shape, a regular auxiliary objective term that minimizes the electrical current consumption of the objective function must be added. The three gradient coils along the x, y, and z configurations were obtained on a sample human-head surface, as shown in Fig. 12. All field inaccuracies were below 0.3% to meet the design requirements. Compared with the calculation results on a cylindrical surface, the coil distributions showed certain similarities, which also verified the design results. The efficiency ($B_{zmax}/|\boldsymbol{I}|$) of the x,

y, and z-gradient coils were 8.248×10^{-5} T/A, 6.075×10^{-5} T/A, and 9.364×10^{-5} T/A, whilst the efficiency of the cylindrical coils at the same scale were 3.499×10^{-5} T/A, 3.499×10^{-5} T/A, and 5.522×10^{-5} T/A. In engineering applications, the current-carrying surfaces of coils can be determined according to actual needs. Flexible coil manufacturing can be used to solve the problem of manufacturing on surfaces.

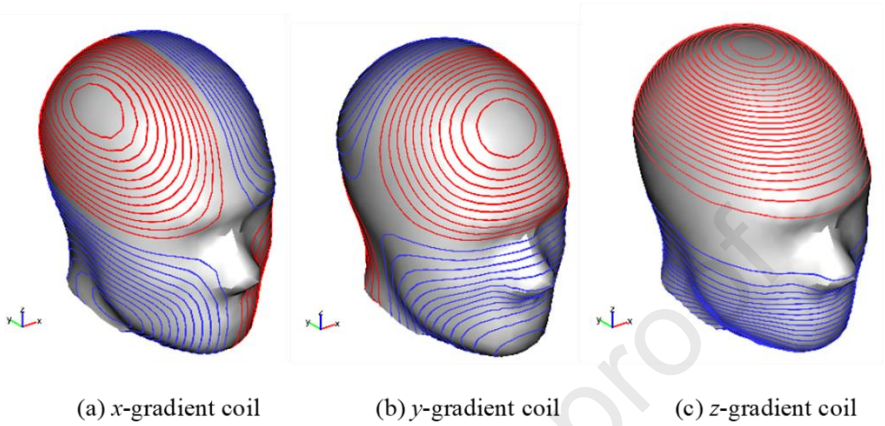

(a) x-gradient coil (b) y-gradient coil (c) z-gradient coil

Fig. 12. Three gradient coils along the x- (a), y- (b), and z- (c) configurations designed using the stream function method on a human-head surface.

4.2 SIMP Method

This method was applied to a spherical surface to obtain the conductive material distribution for microscale MRI gradient coils; these could potentially be used to observe cell or cell clusters, a common task in biological research.

4.2.1 Accuracy verification

The SIMP method, while appropriate for a general surface, can also be applied to a developable surface. The results for a cylindrical surface were compared with the method that develops a cylindrical surface into a plane [11], mainly to verify the accuracy of the calculations. The chosen ROI, size of the current-carrying surface, boundary conditions, and mesh nodes were kept constant. The gradient value was 0.01 T/m. The results of the y-gradient coils were optimized via two methods, as shown in Fig. 13 (1/8 cylindrical surface). After 25 iterations, the changes of objective function value [Eq. (23)] as shown in Fig. 13 (a) and (b), which finally were 0.67621 and 0.67605, respectively. The wire configuration was the same, and the accuracy for the surface gradient, as calculated using the tangential gradient operator, was thus verified.

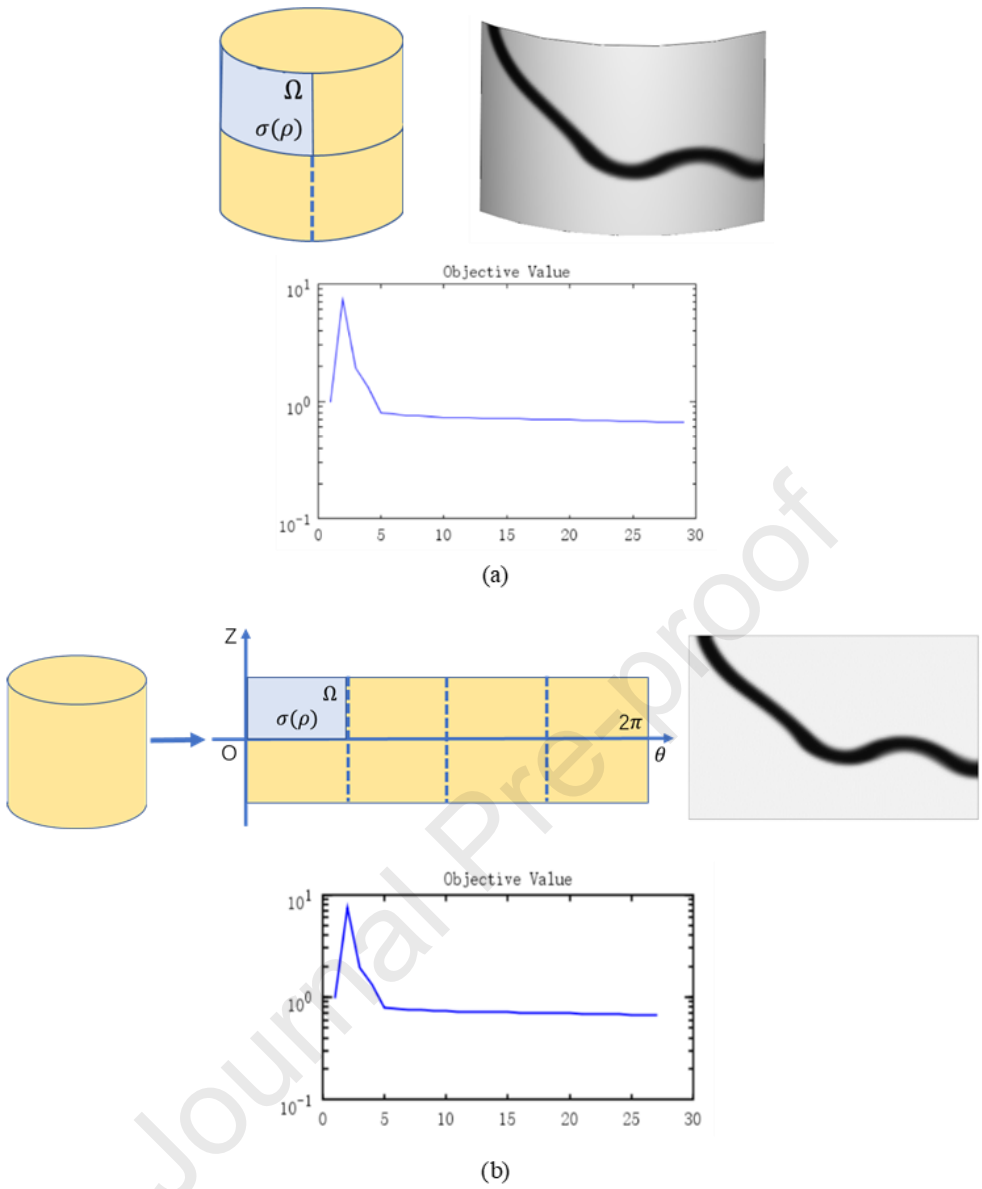

Fig. 13. Comparison of surface and plane optimization results: (a) Optimization results on 1/8 cylindrical surface, obtained using the method described in this article. (b) 1/8 cylindrical surface from an unfolding plane optimization result, as reported in [11].

4.2.2 Spherical surface examples

The optimized design domain for the spherical surface carrying a current was as follows: the spherical surface had a radius of 10 mm, the ROI region was a sphere with a radius of 5 mm, and the gradient value was 0.01 T/m. Because the design domain and ROI were fully symmetrical, the resulting coil shapes were also symmetrical. To improve the calculation iteration speed, the spherical design domain was divided into eight identical subdomains, and only one of the parts was optimized. This made it symmetrical to the other parts, producing a complete wire distribution. For the 1/8 spherical surface, the initial boundary conditions of the x- and z-direction gradient coils are shown in Fig. 14. The y-gradient coil configuration was the same as the *x*-gradient

coil's and only needed to be rotated by 90º.

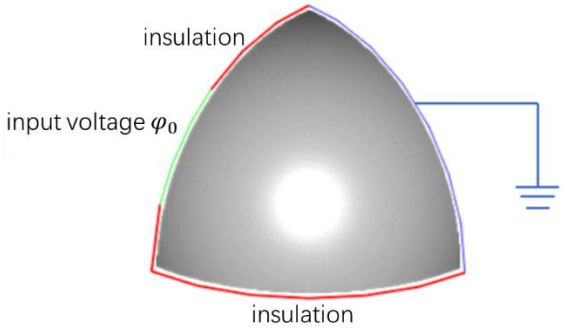

Fig. 14. One-eighth spherical boundary condition.

The triangular mesh of the 1/8 spherical surface mesh was obtained via Delaunay triangulation, as shown in Fig 15. The objective function for the *x*-gradient coils (*y*-gradient coils) and *z*-gradient coils combined the minimum field inaccuracy and maximum coil efficiency (the auxiliary optimization objective can be changed to suit requirements).

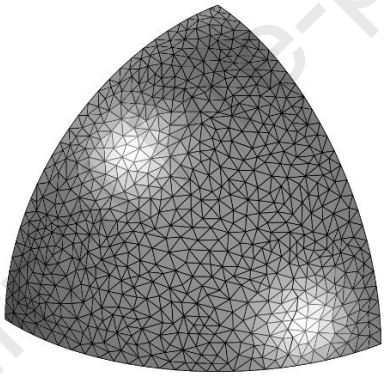

Fig. 15. Delaunay triangulation of 1/8th of the sphere.

The results of the *x*-gradient coil (*y*-gradient coil) configurations for a fully spherical surface are shown in Fig. 16. Fig. 16 (e) shows the gradient field inaccuracy contours for the *x(y)–z* section. The red region indicates an error exceeding 5%. The inaccuracy in the ROI was less than 3.41%, which satisfies the requirements.

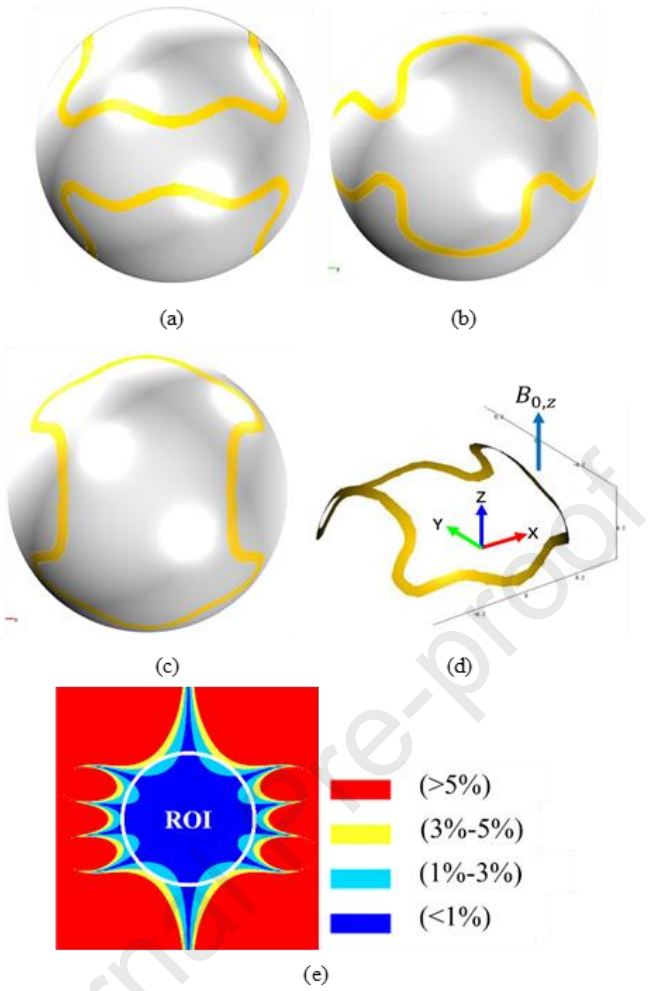

Fig. 16. Optimization results for a spherical surface for *x*- and *y*-gradient coils (the main magnetic field $B_{0,z}$ is in the z direction): (a) *x*–*z*, (b) *y*–*z*, (c) *x*–y, and (d) perspectives of the upper hemispherical coils; (e) the corresponding gradient field inaccuracy contours of the *x*(*y*)-gradient coils in the *x*(y)-*z* section.

The *z*-gradient coils on the fully spherical surface are shown in Fig. 17. Fig. 17 (e) shows the gradient field inaccuracy contours in the *x*–*z* section. The red region indicates an error of more than 5%. The inaccuracy of the gradient magnetic field in the ROI was less than 3.12%, which satisfies the requirements.

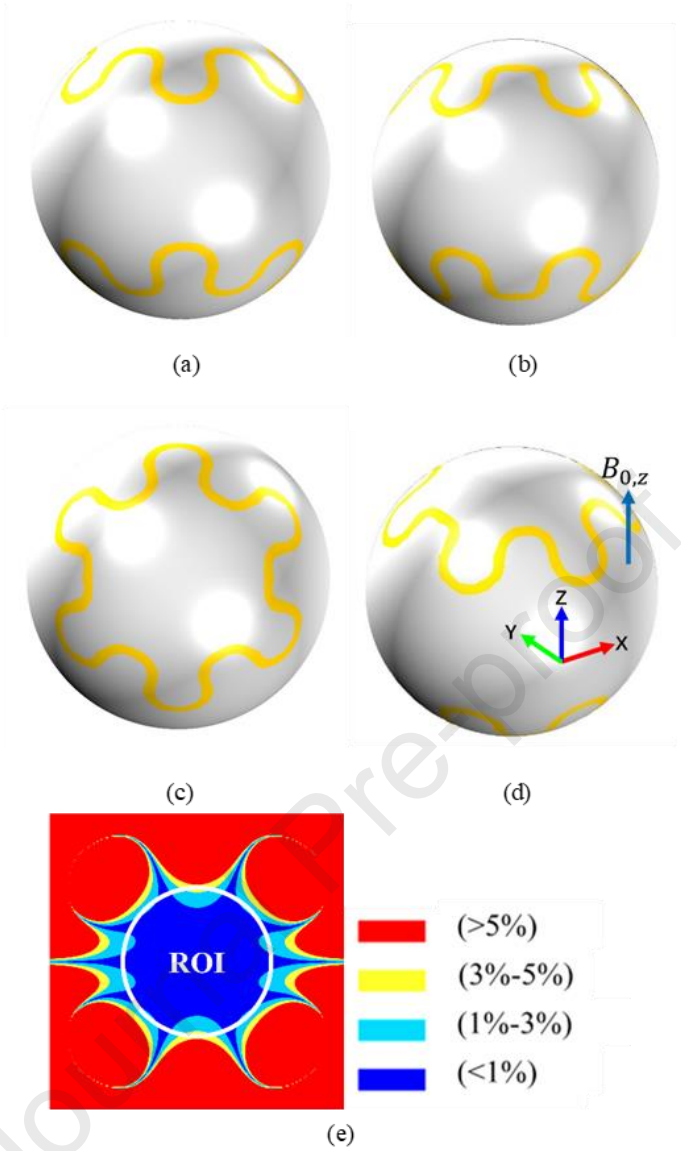

Fig. 17. Optimization results for a spherical surface for *z*-gradient coils (the main magnetic field $B_{0,z}$ is in the z direction): (a) *x*–*z*, (b) *y*–*z*, (c) *x*–*y*, and (d) stereo view of spherical coils; (e) the corresponding inaccuracy gradient field contours of *z*-gradient coils in *x*–*z* section.

5. Conclusions

Calculating the surface normal and electric current or potential for discrete surfaces is critical in gradient coil design methods. The normal vector on a discrete surface is used to calculate the tangential gradient operator. In this study, to achieve geometrical generality, we used a farthest point sampling algorithm to perform Delaunay triangulation on a cloud-point-type current-carrying surface to achieve a convergent geometrical discretization with respect to the mesh size. The numerical examples show that this method can be applied to the two-gradient-coil design methods to obtain an accurate gradient coil configuration on the discretized surface; the results satisfy the design requirements, with an inaccuracy of less than 5%.

CRediT authorship contribution statement

Hao Ren: Methodology, Software->algorithm, Validation, Formal analysis, Investigation, Writing-Original Draft, Visualization. **Hui Pan:** Methodology, Software->algorithm, Formal analysis, Investigation, Data Curation, Visualization. **Feng Jia:** Methodology, Software->algorithm. **Jan G.Korvink:** Conceptualization, Writing-Review & Editing. **Zhenyu Liu:** Conceptualization, Methodology, Software, Resources, Writing-Review & Editing, Supervision, Project administration.

Declaration of competing interest

Jan G. Korvink declares that he is a shareholder of Voxalytic GmbH, a company that produces microscale NMR equipment. The other authors declare that they do not have any commercial or associative interest that represents a conflict of interest in connection with the work submitted.

Appendix A. Supplementary data

Supplementary data to this article can be found online.

Acknowledgment

This research was funded by the National Natural Science Foundation of China under grant No. 51675506. JGK acknowledges support from an EU2020 FET grant (737043 TiSuMR), the Deutsche Forschungsgesellschaft (DFG) (grant KO 1883/20-1 Metacoils), funding within the framework of the German Excellence Initiative under grant EXC 2082 "3D Matter Made to Order", from the VirtMat initiative "Virtual Materials Design", and from an ERC Synergy Grant (951459, HiSCORE).

References

1. R Turner, A target field approach to optimal coil design, 1986, *Journal of Physics D: Applied Physics,* **19** L147
2. R Turner, Minimum inductance coils, 1988, *Journal of Physics E: Scientific Instruments,* **21** 948
3. Forbes L. K., Crozier S. A novel target-field method for finite-length magnetic resonance shim coils, 2001, *Journal of Physics D: Applied Physics,* **34**(24)
4. Hu G., Ni Z., Wang Q., A Superconducting Magnet System for Whole-Body Metabolism Imaging, 2012, *IEEE Transactions on Applied Superconductivity,* **22** 4900604
5. Liu W, Zu D, Tang X, H Guo. Target-field method for MRI biplanar gradient coil design, 2007, *Journal of Physics D: Applied Physics,* **40(15)** 4418
6. Bai Y, Wang Q, Yu Y and Kim K, Target field approach for spherical coordinates, 2004, *IEEE T. Appl. Supercool*., **14** 1317
7. Peeren G N., Stream function approach for determining optimal surface currents, 2003, *Journal of Computational Physics,* **191** 305
8. D. Tomasi, Stream function optimization for gradient coil design, 2001, *Magnetic*

Resonance in Medicine, **45** 505
9. Lemdiasov R. A., Ludwig R., A stream function method for gradient coil design, 2005, *Concepts in Magnetic Resonance Part B Magnetic Resonance Engineering,* **26B** 67
10. Hu Y, Wang Q L, Li Y, Zhu X C and Niu C Q, Optimization of magnetic resonance imaging high-order axial shim coils using boundary element method, *2016, Acta Phys. Sin.,* **65** 218301
11. Hui Pan, Feng Jia, Zhen-Yu Liu, M Zaitsev，J Hennig，JG Korvink, Design of small-scale gradient coils in magnetic resonance imaging by using the topology optimization method, 2018, *Chinese Physics B,* **v.27** 95
12. Sigmund O and Maute K, Topology optimization approaches, 2013, *Struct. Multidisc. Optim.,* **48** 1031
13. Sigmund O., A 99 line topology optimization code written in Matlab, 2001, *Structural and Multidisciplinary Optimization,* **21** 120
14. Deng Y B, Liu Z Y, Zhang P, Liu Y S and Wu Y H, Topology optimization of unsteady incompressible Navier–Stokes flows, 2011, *J. Comput. Phys.,* **230** 6688
15. Dziuk G., Surface finite elements for parabolic equations, 2007, *Journal of Computational Mathematics,* **25** 385
16. Dziuk G, Elliott C M., Finite elements on evolving surfaces, 2007, *Journal of Numerical Analysis,* **27** 262
17. Morvan J M, Thibert B, On the approximation of a smooth surface with a triangulated mesh, 2002, *Computational Geometry: Theory and Applications,* **23** 337
18. J Dai，L Wei，J Miao，Z Wei，H Ying，ST Yau，X Gu, Geometric accuracy analysis for discrete surface approximation, 2007, *Computer Aided Geometric Design,* **24** 323
19. Li H, Zeng W, Morvan J M, Chen L, Gu X, Surface Meshing with Curvature Convergence, 2014, *IEEE Transactions on Visualization and Computer Graphics,* **20(6)** 919
20. Sethian, J. A., A fast marching level set method for monotonically advancing fronts, 1996, *Proceedings of the National Academy of Sciences,* **93** 1591
21. Leibon G, Letscher D, Delaunay triangulations and Voronoi diagrams for Riemannian manifolds, 2000, *Proceedings of the sixteenth annual symposium on Computational geometry*, January 5, 2000, pp. 341-349
22. Gabriel Peyré, Cohen L D, Geodesic Remeshing Using Front Propagation, 2006, *International Journal of Computer Vision,* **69** 145
23. Zhenyu Liu, Feng Jia, Jürgen Hennig, and Jan G. Korvink, Optimization MRI Cylindrical Coils Using Discretized Stream Function with High Order Smoothness, 2012, *IEEE Transactions on Magnetics,* **48** 1179
24. Zhou M and Rozvany G I N, The COC algorithm, Part II: Topological, geometrical and generalized shape optimization, 1991, *Comput. Method. Appl. M.,* **89** 309
25. Bendsøe M P., Optimal shape design as a material distribution problem, 1989, *Structural Optimization,* **1(4)** 193
26. Soares C A M, 1987, *Computer Aided Optimal Design: Structural and Mechanical*

Systems (Heidelberg: Springer) pp. 271–311
27. Svanberg K, The method of moving asymptotes – a new method for structural optimization, 1987, *Int. J. Numer. Meth. Eng.,* **24** 359
28. O. Sigmund, J. Petersson, Numerical instabilities in topology optimization: A survey on procedures dealing with checkerboards, mesh-dependencies and local minima, 1998, *Structural Optimization,* **16** 68
29. F. Jia, Z. Liu, M. Zaitsev, J. Hennig, J. Korvink, Design multiple-layer gradient coils using least-squares finite element method, 2014, *Structural and Multidisciplinary Optimization,* **49(3)** 523

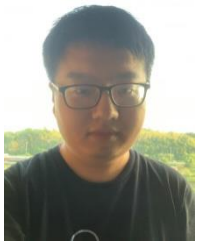

Hao Ren received his B.S. degree in mechanical engineering from Hunan University, Changsha, China. He obtained the master's degree in mechanical engineering from University of Chinese Academy of Sciences. Now he is a doctoral student in Nagoya Univerity, Japan. His research interests are numerical simulation and topology optimization.

Jan G. Korvink received the M.Sc. mech. degree from the University of Cape Town in 1987, and the Dr. sc. techn. degree from ETH Zurich in 1993. In 1997 he became full professor of Microsystems Engineering at IMTEK at the Albert Ludwig University in Freiburg, Germany, and in 2015 he moved to the Karlsruhe Institute of Technology to head the Institute of Microstructure Technology. In 2011 he received an ERC Advanced Grant, and in 2021 he received an ERC Synergy Grant, both from the European Research Council. In addition, his research has enjoyed funding from within the Excellence Initiative of the German Government. His current research focuses on MEMS applications in Magnetic Resonance, and novel techniques in Added Nanomanufacturing.

Zhenyu Liu received his Ph.D. degree in mechanical engineering from Dalian University of Technology, Dalian, China, in 2000, and his Habilitation in microsystems from the Department of Microsystems Engineering, University of Freiburg, Freiburg, Germany, in 2009. Since 2009, he has been a Professor in Changchun Institute of Optics, Fine Mechanics and Physics (CIOMP), Chinese Academy of Sciences, Changchun, China. His research interests are the simulation and design and fabrication of devices in MOMES.

Supporting Information

Accurate surface normal representation to facilitate gradient coil optimization on curved surface

Hao Ren [a, b], Hui Pan [b], Feng Jia [c], Jan G. Korvink [d, *], Zhenyu Liu [a, **]

[a] *Changchun Institute of Optics, Fine Mechanics and Physics, Chinese Academy of Sciences, Changchun, 130033, China*
[b] *School of Optoelectronics, University of Chinese Academy of Sciences, Beijing, 101499, China*
[c] *Department of Radiology, Medical Physics, Medical Center University of Freiburg, Faculty of Medicine, University of Freiburg, Freiburg, 79110, Germany*
[d] *Institute of Microstructure Technology, Karlsruhe Institute of Technology (KIT), Karlsruhe, 76049, Germany*

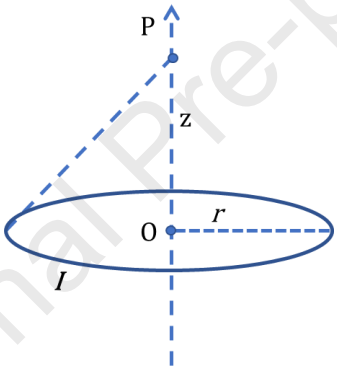

Fig. S1. Magnetic induction on the central axis of a current-carrying ring.

A current-carrying ring with electrical current I, and magnetic induction at a point P directly above its center O is (**Fig. S1**):

$$B_z = \frac{\mu_0 r^2 I}{2(r^2+z^2)^{3/2}}. \quad \text{(Eq. S1)}$$

Here B_z is the magnetic induction at a point P, *r* is the radius of the ring, z is the length of the line **OP**, and μ_0 is the permeability of vacuum. Accordingly, the magnetic induction at the center of the current-carrying sphere surface can be derived (see Fig. S2.).

* Corresponding author.
** Corresponding author.
E-mail addresses: jan.korvink@kit.edu (J. Korvink), liuzy@ciomp.ac.cn (Z. Liu).
Peer review under responsibility of Innovation Academy for Precision Measurement Science and Technology (APM), CAS.

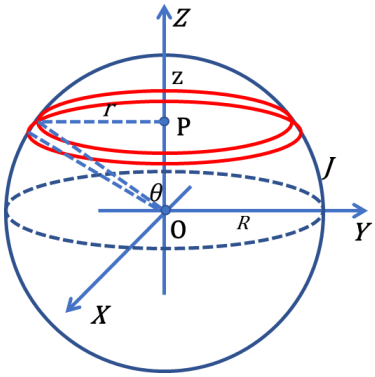

Fig. S2. Magnetic induction at the center of the current-carrying spherical surface.

Let $\psi = \alpha z$ on the surface, α being a constant. The magnetic induction B_z is obtained at point **O**:

$$B_z = \frac{\alpha}{3}\int_0^{\pi} \mu_0 \sin^2\theta \cdot J \mathrm{d}\theta = \frac{\alpha}{2}\int_0^{\pi} \mu_0 \sin^3\theta \, \mathrm{d}\theta$$

$$= \frac{2}{3}\alpha\mu_0. \qquad \text{(Eq. S2)}$$